iScience

CellPress
OPEN ACCESS

Article

A crack compensation strategy for highly stretchable conductors based on liquid metal inclusions

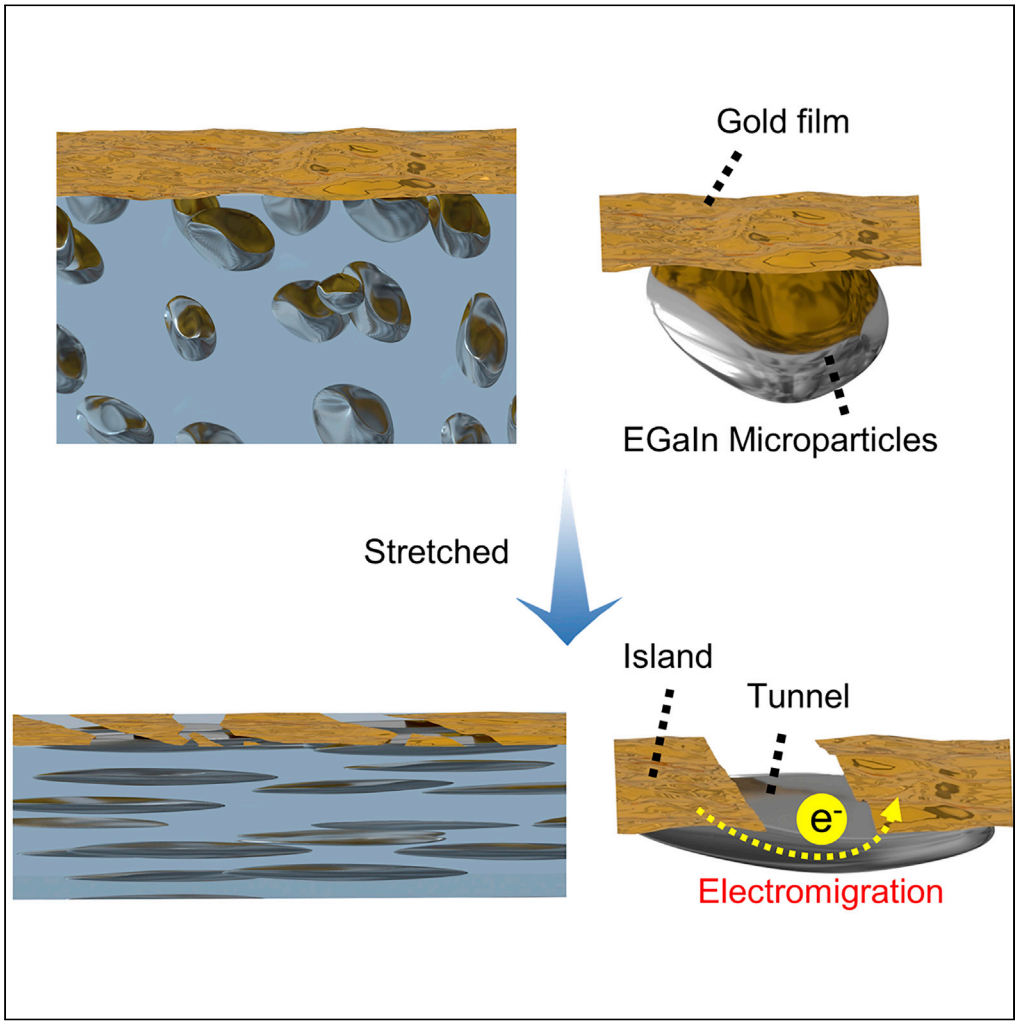

Guoqiang Li, Xing Ma, Zirong Xu, ..., Zhiwu Xu, Shi-Yang Tang, Zhiyuan Liu

maxing@hit.edu.cn (X.M.)
s.tang@bham.ac.uk (S.-Y.T.)
zy.liu1@siat.ac.cn (Z.L.)

Highlights

Our crack compensation strategy enhances the performance of a stretchable conductor

Liquid metal microparticle inclusions can be stretched to connect the cracked Au film

The conductor can be stretched up to 260% strain with negligible resistance change

The conductor shows great potential for *in vivo* and *in vitro* biomedical applications

Li et al., iScience *25*, 105495
December 22, 2022 © 2022 The Author(s).
https://doi.org/10.1016/j.isci.2022.105495

iScience

CellPress
OPEN ACCESS

Article

A crack compensation strategy for highly stretchable conductors based on liquid metal inclusions

Guoqiang Li,[1,3] Xing Ma,[1,5,*] Zirong Xu,[4] Yifeng Shen,[1] Man Yuan,[1] Jianping Huang,[2] Tim Cole,[3] Jingjing Wei,[2] Sanhu Liu,[4] Fei Han,[2] Hanfei Li,[2] Bayinqiaoge,[3] Zhiwu Xu,[4] Shi-Yang Tang,[3,*] and Zhiyuan Liu[2,*]

SUMMARY

Crack control strategies have been proven very useful for enhancing the stretchability of metal film-based stretchable conductors. However, existing strategies often suffer from the drawbacks of complicated preparation and predefined effective directions. Here, we propose a crack compensation strategy for preparing conductors featured with high stretchability by using liquid metal microparticles (LMMPs)-embedded polydimethylsiloxane (PDMS) as the substrate with a thin film of gold (Au) sputtered on the surface. LMMPs can be elongated to connect the cracked Au film upon stretching, which can form a conductive "island-tunnel" (IT) architecture to compensate for the cracks and maintain the conductivity. The high performance of the stretchable conductor is demonstrated by using it as electrodes to record surface electromyography of human brachioradialis and monitor electrocorticography signals of a rat in normal and epileptic states. The developed strategy shows the potential to provide a new perspective for the fabrication of flexible electronics.

INTRODUCTION

The development of high-performance metal film-based stretchable conductors plays a crucial role in advancing the fabrication of scalable and stable flexible electronic devices which can be endowed with versatile electronic functions of sensing,[1–3] display,[4–6] energy harvesting[7,8] and so on. Metal film-based stretchable conductors are a crucial component that can be patterned on a flexible substrate to form flexible circuits, thereby addressing the common problem of interfacing mismatch between a curvilinear surface and conventional rigid electronics. However, cracks in the metal film will be generated due to the strain transferred from the stretchable polymer substrate, this greatly increases the electrical resistance and can even induce electrical disconnection.[9] Therefore, stretching metal film-based conductors to large strain while maintaining a low resistance is one of the major challenges in stretchable electronics.[3,10,11]

One strategy for addressing this problem is to cut rigid materials with very thin thickness into specific structures such as serpentines,[12] waves,[13] helices,[14] and meshes.[15,16] However, the conductors prepared based on "spring principles" can only offer overall but not local stretchability, which could lead to irreversible damage under large deformation (>100%). Alternatively, the method based on controlling the microstructure of the deposited metal film on a compliant substrate has been extensively explored to maintain the conductivity upon stretching.[5,17–19] In addition, measures such as adding an adhesion layer between the metal film and the elastic substrate,[6,20,21] designing specific microstructures on the surface of the substrate,[11,22,23] and pre-stretching the substrate[24,25] have been widely reported as crack control strategies. These methods may be effective, but they require extra processes that lead to complicated fabrication. Also, limited stretchability and direction-dependent effectiveness of the crack control strategy are regarded as additional drawbacks.[26] A large change in conductivity at a high load strain will lead to inaccurate electrical signals and functional failure of devices, which puts forward a requirement for more advanced crack compensation strategies.

Recently, gallium (Ga)-based liquid metals (LMs) have been demonstrated to possess promising prospects for use in flexible electronics owing to their intrinsic fluidity and metallic conductivity.[27–30] For instance, Stéphanie and co-workers developed an intrinsically stretchable biphasic (solid-liquid) thin metal film with

[1]Sauvage Laboratory for Smart Materials, School of Materials Science and Engineering, Harbin Institute of Technology (Shenzhen), Shenzhen 518055, China

[2]Research Center for Neural Engineering, Shenzhen Institute of Advanced Technology, Chinese Academy of Sciences, Shenzhen 518055, China

[3]Department of Electronic Electrical and Systems Engineering, University of Birmingham, Edgbaston, Birmingham B15 2TT, UK

[4]State Key Laboratory of Advanced Welding and Joining, Harbin Institute of Technology, Harbin 150001, China

[5]Lead contact

*Correspondence: maxing@hit.edu.cn (X.M.), s.tang@bham.ac.uk (S.-Y.T.), zy.liu1@siat.ac.cn (Z.L.)

https://doi.org/10.1016/j.isci.2022.105495

This is an open access article under the CC BY-NC-ND license (http://creativecommons.org/licenses/by-nc-nd/4.0/).

excellent stretchability and conductivity prepared by the vapor phase deposition of LM on an Au film.[26] This kind of thin metal film can be easily stretched up to 400% strain with a relatively low resistance change ($\Delta R/R_0 \approx 20$) attributed to the continuous biphasic (liquid-solid) phase. Nevertheless, relatively bulky LM droplets still present a risk of leakage, and the biocompatibility of the intermetallic $AuGa_2$ compound is uncertain. In addition to stretchable conductors that are fabricated from bulk LMs, the use of LM-elastomer composites for fabricating conductors with high reliability has been extensively studied,[31–33] which leaves ample space for enhancing the stretchability of metal films using LMs.

Herein, we present an efficient crack compensation strategy for the fabrication of stretchable conductors with "island-tunnel" (IT) architectures prepared by sputtering a layer of Au thin film onto a LMMPs-PDMS composite. Different from the commonly used crack control strategy, the stretchability of the Au film conductor is enhanced by compensating conductive pathways underneath the cracks in this work. Attributed to the fluidity of LMs, the LMMPs underneath can be stretched from a "spherical" shape to a "rod" shape and act as the "tunnels" to compensate for the cracked Au films (islands). Therefore, the developed conductor can maintain an insignificant resistance variation (R/R_0 is about 7.1) before breaking at ~260% strain. Making full use of these outstanding properties, we successfully used the stretchable conductor for the on-skin detection of surface electromyography (sEMG) signals of the brachioradialis and achieved artificial intelligence (AI) enabled hand gesture recognition. We also show that stretchable circuits can be patterned by using a designed shadow mask for sensing electroencephalogram (ECoG) signals of a rat. The successful demonstrations of the applications are attributed to the high stable conductivity of the developed conductor endowed by the LMMPs compensating role.

RESULTS AND DISCUSSION

Schematic of the crack compensation strategy

Inspired by subsea tunnels which play the function of connecting islands on both sides of a strait and serving as a passage for vehicles (Figure 1A), we introduced conductive pathways to compensate cracks generated on an Au film upon stretching. Therefore, IT architectures by depositing Au nanofilm onto the LMMPs-PDMS composite substrate were proposed to fabricate stretchable conductors with enhanced stretchability. The conductive mechanism of our conductor is similar to the function of a subsea tunnel. The Au film and LMMPs respectively play the role of the land on both sides and the tunnel, which allows for the passage of electrons (i.e., vehicles in Figure 1A) (Figure 1B). When stretched (Figure 1C), the rigid Au film will crack due to the mechanical mismatch of the interface between the Au film and the elastomer substrate, and the crack length is positively correlated with the conductor strain. Furthermore, the cracked Au film will become nonconductive once a penetrating crack is perpendicular to the tensile direction. Fortunately, LMMPs in the elastomer substrate can be stretched from a "spherical" shape to a "rod" shape owing to the intrinsic deformability of LM. The "rod" shaped LMMPs act as "tunnels" close to the surface of the elastomer substrate that can compensate for the crack and connect the Au films (islands). We also simulated the voltage distribution based on the obtained SEM image (Figure 1B) to show its electrical conductivity referring to previously reported results.[2,22,34] We retained (Figure 1D) and removed (Figure 1E) the LMMPs shown in the SEM image by image processing, and the voltage distribution is simulated by applying a 1 V voltage drop on both sides. It clearly shows that the voltage of the conductor with LMMPs drops gradually, while the conductor without LMMPs is an open circuit. In contrast to the crack control strategy, the stretchable conductor developed here relies on a native microstructure design using LMMPs to compensate for the cracks. The IT architecture plays an essential role in enhancing the conductive performance due to the synergistic effect of the rigid Au film and deformable LMMPs. Additionally, suspending LM into a PDMS matrix as microparticles prevents the leakage of LM and improves the reliability of the conductor.

Preparation and characterization of the stretchable conductor

The fabrication process for creating the highly stretchable and electrically stable conductor with IT structure is shown in Figure 2A. We first mixed EGaIn and PDMS with a volume fraction ratio of 2:3, then stirred to rupture the bulk LM into microparticles until the LMMPs were uniformly dispersed in the PDMS matrix. We next cured the LMMPs-PDMS composite at 70°C for 3 h and sputtered a nanolayer Au film onto its surface. A more detailed fabrication process is given in the method details. Our method of encapsulating LMMPs inside the PDMS elastomer not only retains the deformability of LMMPs on a microscale but also avoids the possibility of bulk LM leaking from the encapsulating polymer. Combined with the deposited Au film, a highly stretchable and reliable conductor endowed with the IT architecture is achieved.

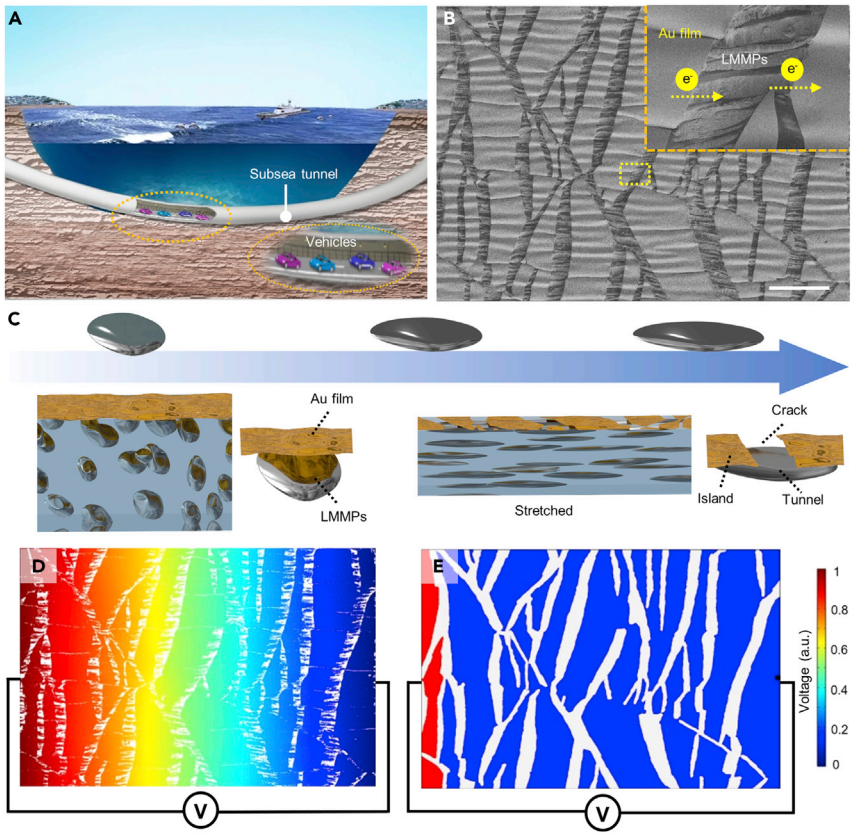

Figure 1. The proposed concept of the stretchable conductor with high stretchability as endowed with an "island-tunnel" architecture

(A) Diagram showing the model of a subsea tunnel connecting the mainland on two sides of a strait, serving as a passage for vehicles.

(B) SEM image of the conductor under 40% strain. The Au film and LMMPs correspond to the mainland and subsea tunnel in (A), respectively. Based on this microstructure design, the electrons (vehicles) can migrate regardless of the Au cracks. Scale bar is 100 μm.

(C) Illustration of the morphology of LMMPs and Au film before and after being stretched.

(D and E) Voltage distribution simulation based on the obtained SEM image of (B) by remaining and eliminating LMMPs, respectively. The result showing a rapid voltage drop when the LMMPs are eliminated indicates electrical disconnection.

An elastomeric composite made by mixing LM with PDMS (1:1 ratio by volume) can become conductive after being compressed by a thin-tipped tool.[35] Therefore, we prepared the composite with less LM (20 and 40% volume fractions) to avoid the substrate becoming conductive due to external compression. Back-scattered electron (BSE) images of the composite with different volume fractions of LM and LMMPs sizes are shown in Figures 2B and S1. The LMMPs are uniformly dispersed in the PDMS matrix, and the distance between the two particles is more than 1 μm. There is no conductive network formed and the LMMPs-PDMS composite is nonconductive as shown in Figure S2. Moreover, we observed diffuse reflections on the composite surface, indicating that the surface is rough. The surface topography was characterized, as shown in Figures 2C and S3, in which we can see that the surface of LMMPs-PDMS substrate is much rougher as compared to the smooth surface of PDMS. Furthermore, the roughness increases with the increase of the LM volume fraction and LMMPs size, as indicated by the arithmetical mean height (Figure S4). We believe that there is a thin layer of PDMS film on the surface of the uppermost LMMPs of the composite. In addition, energy dispersive X-ray spectroscopy (EDS) element mapping and spot analysis (Figure S5) of the LMMPs-PDMS composite further demonstrate the existence of silicone on the surface of the uppermost LMMPs. Furthermore, we quantified the thickness of the PDMS film on the LMMPs surface by atomic force microscopy (AFM) force-displacement measurement by using In particle (solid at room temperature) to replace the LMMPs. After the AFM tip was lowered to touch the LMMP surface, a gradually increasing repulsive force was detected. However, the tested results are not entirely consistent for different

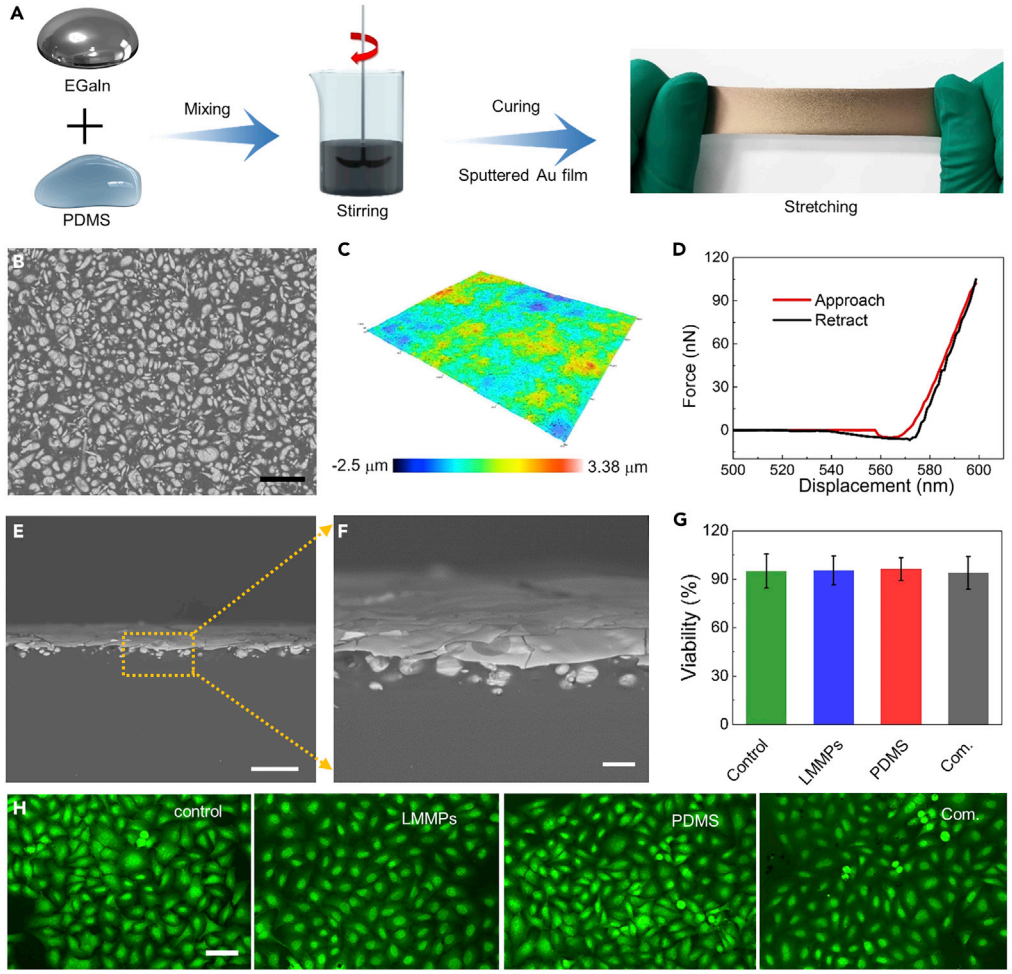

Figure 2. Preparation of the stretchable conductor and characterization of its microstructure

(A) Preparation process and photo of the stretchable conductor.

(B) BSE image of PDMS-LMMPs substrate with 40% volume fraction of LM. LMMPs with an average diameter of 7.5 μm are uniformly dispersed in the PDMS matrix. Scale bar is 40 μm.

(C) Surface topography of the substrates indicates the rough surface.

(D) Force-displacement curve of one tested point, the red line, and blue line present the approach process and retraction process between the AFM tip and the LMMP, respectively.

(E and F) BSE characterization of the cross-section morphology of the stretchable conductor after sputtering Au film, (F) is the partially enlarged image. Scale bars are 40 and 10 μm, respectively.

(G) Quantification of HEK-293 cell viability that grown on the control sample, LMMPs, PDMS, and PDMS-LMMPs composite. Error bars show SD N = 6.

(H) Fluorescent image of stained living cells co-cultured with different samples. Scale bar is 50 μm. See also Figures S1 and S3–S7.

points. The approaching force-displacement curves of some tested points are similar to the reference sample indicating a very thin PDMS film (~5 nm, Figure 2D). In comparison, some other approaching force-displacement curves with two distinct slopes obviously (Figure S6B) indicate a thicker PDMS film.

After the "tunnel" architecture of the conductor in the LMMPs-PDMS composite substrate was built, a thin Au film layer that plays the role of "island" was then deposited by sputtering. As shown in Figures 2E and 2F, the Au film completely covered the rough surface of the substrate, and many cracks were introduced during the sample preparation process due to the rigid and fragile mechanical properties of the deposited Au film. Moreover, the biocompatibility of the material is of paramount importance for wearable and *in vivo/vitro* applications. To test the biocompatibility of the LMMPs-PDMS composite, we

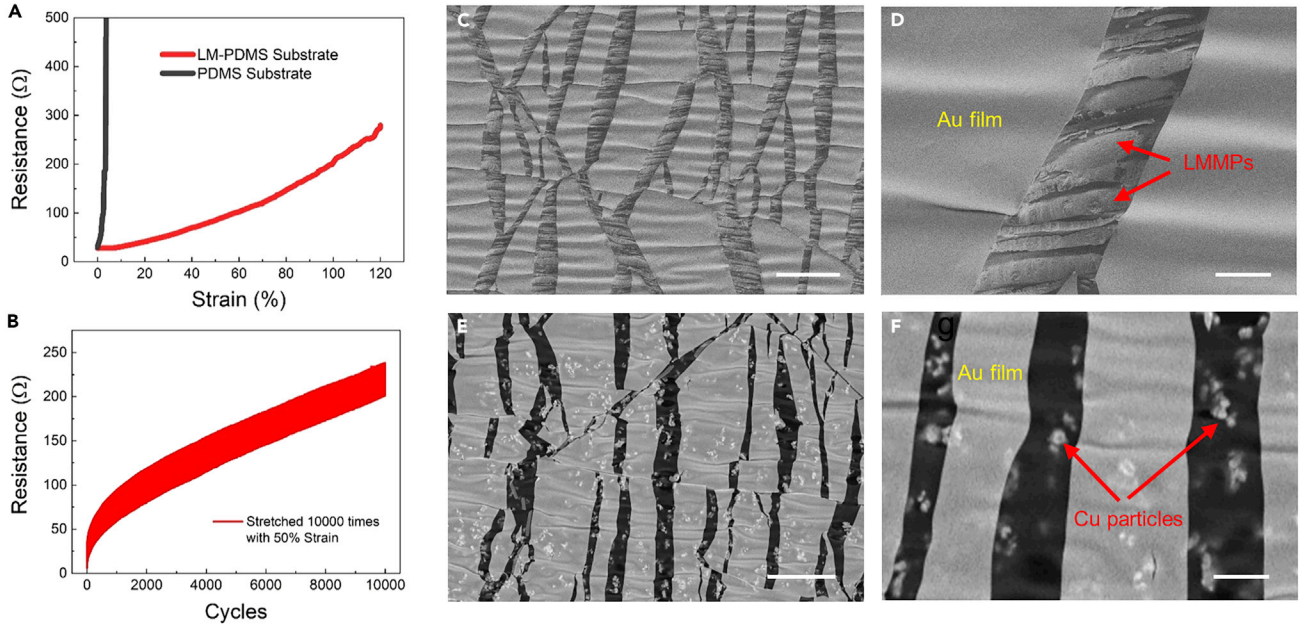

Figure 3. Electromechanical performance and microstructure evolution of the stretched conductor

(A) Resistance changes of conductors prepared by sputtering Au film on PDMS and LMMPs-PDMS composite substrates, respectively.

(B) Long-term stability test of the stretchable conductor under 50% strain.

(C and D) Microstructure characterization of the stretchable conductor (40 vol%-7.5 μm) with IT architecture under 40% strain, indicating the "tunnel" role of LMMPs to compensate for the cracks.

(E and F) SEM image of the conductor with CuMPs-PDMS composite substrate with 20 vol % rigid Cu particle cannot connect the cracked Au film. See also Figures S12–S15.

carried out the live/dead-staining on HEK-293 cells grown on various samples. All results show the cell viability of ~96% after 24 h suggesting high biocompatibility (Figure 2G). Fluorescent images shown in Figure 2H further verify a regular cell morphology with serried live cells, and the corresponding bright-filed images are shown in Figure S7. These results are consistent with previous results,[36] which prove the excellent biocompatibility of the LMMPs-PDMS-based stretchable conductor.

Investigating the mechanism of the compensation strategy

The electromechanical response was evaluated to investigate the effects of the crack compensation strategy on the electrical performance of the studied stretchable conductor with IT architectures. As shown in Figure 3A, the conductor (40 × 30 mm size) with IT architectures can be stretched over 260% strain, resulting in an increase of resistance by ~7.1 times. In addition, the tensile limit of the LMMPs-PDMS composite is enhanced and the elastic modulus decreases owing to the LMMPs addition (Figure S8).[35,37] In comparison to the excellent performance of the stretchable conductor with the IT architecture, an open circuit occurred for a sample with only Au film sputtered on PDMS upon the application of 3% strain. To examine the effect of the thickness of the LMMPs-PDMS substrate on the electromechanical performance, we deposited Au films (thickness of 40 nm) on LMMPs-PDMS substrates of various thicknesses (0.5, 1.0, and 2.0 mm). Our results suggest that the thickness of the substrate has no obvious effects on the electromechanical performance (Figure S9A). In addition, we deposited Au films with different thicknesses (20, 40, and 80 nm) on a 1.0 mm thick substrate to investigate the influence of the Au film thickness on the electromechanical performance (Figure S9B). Our results show that the R/R_0 of the case with 20 nm Au film thickness is about 4 times higher than the other two cases under ~260% tensile strain. Therefore, considering the material cost and fabrication efficiency, we choose 40 nm as the Au film thickness. Furthermore, when compared to surface conductive conductors with an Au film coating that can reach a resistance of hundreds of ohms after long-term cyclic stretching tests,[2,18,23,38,39] the resistance of our conductor is below 100 Ω after 10,000 times of stretching (Figure 3B), suggesting its outstanding electromechanical performance. To understand the cause of the increase in resistance, we monitored the microstructure of the conductor surface during the cyclic test, as shown in Figure S10. The density of cracks increased after repeatedly stretching, leading to an increase in the resistance. Figure S11 compares the electromechanical performance of the

conductor developed in this work with previously reported LM-embedded and Au film-coated elastomeric conductive composites. Although LM-embedded composite conductors offer higher stretchability and lower resistance variation, the conductor prepared based on our compensation strategy are surface conductive and more biocompatible. Besides, compared with other Au film-coated conductors, our LMMPs compensation strategy significantly improves the electromechanical performance.

To further understand the mechanism of the ability to maintain conductivity when using LMMPs-PDMS as the stretchable substrate, the surface microstructure of the conductors under strain was investigated. For a PDMS substrate with an Au film coating, dense and parallel cracks are easily formed when the conductor is under a small strain due to the mechanical mismatch of the interface between the Au film and PDMS (Figure S12). For the conductor prepared by sputtering Au film on a LMMPs-PDMS substrate, cracks (width varying from 20 to 50 μm) were also formed and aligned perpendicular to the stretched direction. Meanwhile, dense LMMPs are elongated and compensate for the crack (Figures 3C and 3D, and Video S1). During the stretching process, we found that a few LMMPs can be ruptured and react with the Au film, as shown in Figure S13A. According to the EDS measurement (Figures S13B and S13C), the formed alloy should be $AuGa_2$.[26] The formation of alloy only occurred near the cracks, and no formation of the Au-Ga alloy was observed in other regions. Therefore, the conductive pathways are formed by LMMPs (tunnel) and the Au film combined with a small portion of alloy near the edge of cracks. The consumption of Au and Ga to form $AuGa_2$ alloy has little effect on the conductor's performance. To further verify our hypothesis, we designed a CuMPs-PDMS composite as the substrate to understand the effect of rigid particles on the response to strain. As given in Figures 3E and 3F, and Video S2, rigid CuMPs cannot be deformed to connect the Au films, and the resistance response vs. strain is similar to that of the Au film deposited on a PDMS substrate, as shown in Figure S14.

The conductivity performance of the conductor is greatly enhanced by using LMMPs-PDMS composite as the stretchable substrate. The LMMPs-PDMS composite and cracked Au film are all nonconductive (Figures S2 and S12). However, flexible LMMPs can be stretched to compensate for the cracked Au film and therefore form the conductive pathways. It should be noted that there is a thin PDMS film of several nanometers of thickness between the LMMP and Au film (Figure 2D). Previous reports suggest that Au atoms can penetrate into the polymer during the deposition process,[40,41] which explains that the conduction mechanism could be attributed to the tunneling effect.[42–44] In addition, the conductivity performance of the conductor is related to the LM volume fraction and LMMPs diameter (Figure S15). The higher density of LMMPs corresponds to more IT architectures, and a rougher surface means that there are more LMMPs on the PDMS substrate surface to be in contact with the Au film. Among all the tested samples, we found that the conductor prepared by a substrate with a 40% volume fraction of LM and an average LMMP diameter of 7.5 μm provides the best conductive performance.

Based on the crack compensation strategy, the electrical performance of the Au film is significantly enhanced. In addition, using the LMMPs-PDMS composite as the conductor substrate not only retains the flexibility of LMMPs but also limits the fluidity of LM, which reduces the risk of LM leakage for wearable and biomedical applications (Video S3). Compared with previously reported LMMPs-PDMS composites which are internally conductive,[35,45] the conductive pathways of our stretchable conductor can be built on the surface attributed to the "island-tunnel" architectures. A few works reported that the composite can be surface conductive after the laser or friction sintering process to expose the internal LM particles.[46,47] However, exposed LM can easily contaminate other surfaces and compromise the stability of conductivity after repeated use. Besides, the reported LM-elastomer composites require a high-volume content >50 vol % to be conductive after sintering,[35] while our method only needs 20 vol % of LM and can offer comparable electromechanical properties. Moreover, our method avoids the concerns of the toxicity of LMs as Au film has been clinically proven with excellent biocompatibility.[3,27,48]

Applications of the stretchable conductor

Surface electromyography (sEMG) monitoring has attracted much attention in sports health monitoring, human-machine interfaces, soft robotics, and prosthesis control.[49–53] Wet electrodes prepared based on rigid metals and conductive gels have been conventionally used for sEMG recording but cannot fully satisfy the requirements due to skin allergy and motion artifact problems.[54] In comparison, dry flexible electrodes are a promising alternative for sEMG monitoring that can overcome the two problems mentioned above.[55,56] The studied stretchable conductor in this work with high electrical stability, excellent

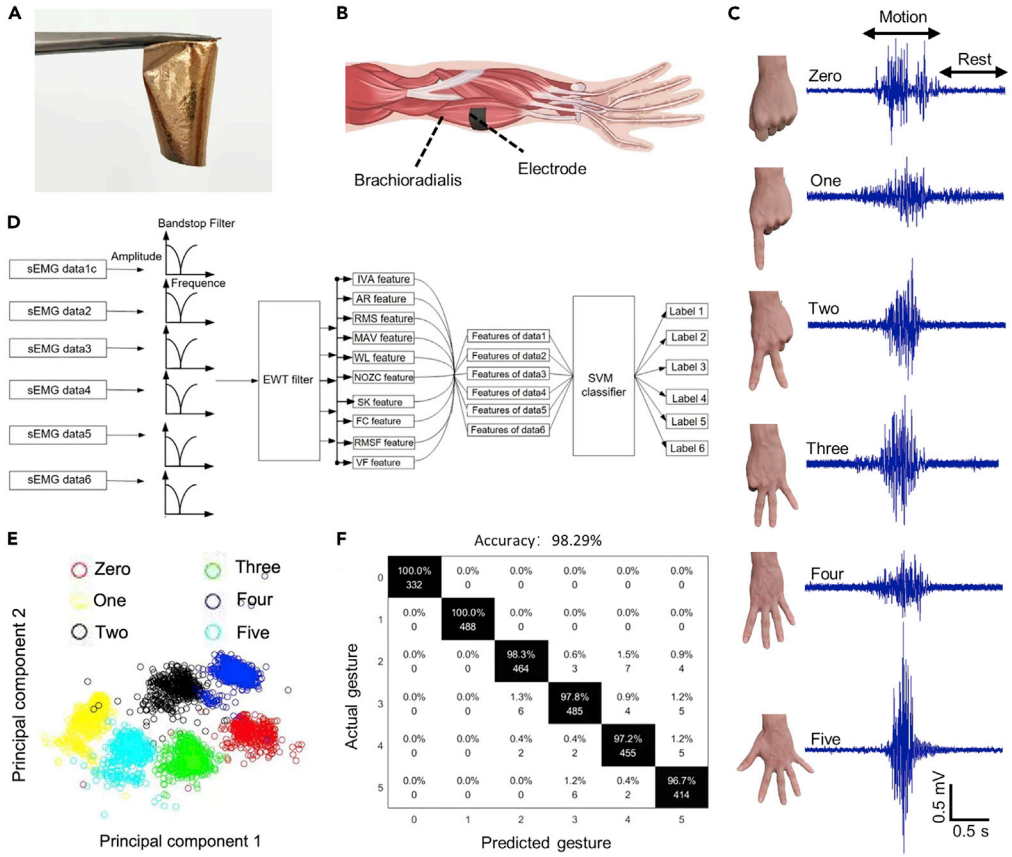

Figure 4. Demonstration of the conductor for sEMG sensing and hand gesture recognition based on machine learning

(A) Photograph of the sEMG electrode.

(B) The electrode was applied to detect the sEMG signal of brachioradialis.

(C) The waveforms recorded from the sEMG sensing electrode corresponding to the hand gestures.

(D) The algorithm logic illustration diagram of the machine learning of hand gestures.

(E) Principal component analysis of the recorded sEMG signals.

(F) Classification confusion matrix for the predicted results, white and black text values are percentages of correct and incorrect predictions, respectively. See also Figure S17.

biocompatibility, and lower elastic modulus is an excellent candidate for sEMG monitoring. The electrochemical properties of the sEMG electrode (Figure 4A, ~60 μm thickness) were tested using electrochemical impedance spectroscopy in phosphate buffered saline (PBS) solution (Figure S16). The result shows a slight increment with increased strain at 100 Hz, which is vital for stable and high-quality signal recording. We used medical air-permeable tape to attach the electrode onto the skin to monitor the sEMG of brachioradialis (Figure 4B) for six hand gestures. For the detected sEMG signals (Figures 4C and S17), electrical activities corresponding to the six gestures detected from the brachioradialis can be easily recognized, and all of the sEMG signals have a high signal-to-noise ratio. As shown in Video S4, in the resting state, the sEMG signal is a straight line. Signal fluctuations were observed when fingers are bent. Such high-quality sEMG signals are mainly attributed to the high electrical stability and stable contact between the electrode and the arm skin.

Additionally, we applied sEMG signals of the six hand gestures to machine learning for hand gesture recognition. Firstly, we improved the signal-to-noise ratio by filtering out fixed-frequency interference based on band-stop filtering.[57] It is necessary to filter the fixed-frequency interference on the collected signal due to the interference of the sEMG signal introduced by electric and magnetic fields. In the time-domain signal of sEMG, high-frequency noise will directly affect the expression of the integral signal. Therefore, we used empirical wavelet transform to filter the detected high-frequency signals, and

the overall signal expression was retained without high-frequency interference (Figure 4D).[58] However, the signal still contains much redundant information after filtration. It is challenging to recognize the six sEMG signals when directly inputting them into a pattern recognition algorithm.[59] Therefore, we first extracted 10 eigenvalues, including the time domain and frequency domain to characterize the integral properties of the detected signals. To demonstrate the effectiveness of the feature extraction process, we used the principal component analysis (PCA) algorithm to perform a dimensionality reduction visual analysis on the extracted 10 eigenvalues. As shown in Figure 4E, the intra-class differences are insignificant and the inter-class differences are apparent, indicating that 10 eigenvalues are feasible to characterize the overall attributes of the original signals.

Support vector machine is a supervised pattern recognition method, which has been widely used in image recognition, industrial detection, and fault monitoring. We used the radial basis function to perform pattern classification on the extracted 10 features under different hand gestures. From the visualization results of the test given in Figure 4F, the overall classification accuracy is 98.29%, and all the intra-class classification accuracies are above 98%. The high classification accuracy demonstrates that it is feasible to apply the stretchable conductor for hand gesture recognition based on the detected sEMG signals.

The developed stretchable conductor has been demonstrated with good performances in electromechanical response and the capability of sEMG signal detection. Circuits with specific patterns can also be fabricated by covering a shadow mask on the top of the LMMPs-PDMS composite substrate during the sputtering process (Figure 5A). A customized circuit pattern under a stretching state is shown in Figure 5B, only the area with sputtered Au film (with IT architectures) is conductive and the other substrate parts are nonconductive. We demonstrated that a stretched circuit with a 1.5 mm width and 20 mm length patterned on the LMMPs-PDMS substrate can easily light a LED, while the LED is off if the circuit is patterned on the PDMS substrate under a small strain (Figure S18). Most importantly, the robustness of the circuit prepared by this method is greatly improved compared with a raw liquid metal circuit (Video S3), meaning the risk of LM leakage and short circuit are significantly reduced. However, being different from the conductors for testing electromechanical response (see Figure 3A) and recording sEMG signals (see Figure 4A) with large areas of Au film, the sputtered narrower Au circuit with less IT architectures leads to higher resistance. The resistance of the patterned 30 mm-length circuits with different widths under 0%, 25%, and 50% strains was tested (Figure 5C). The wider circuits correspond to lower resistance, and this phenomenon is mainly owing to the fact that more IT architectures in wider circuits provide more pathways for electrons. Therefore, appropriately increasing the circuit width can further reduce the resistance, but this circuit patterning strategy is not applicable for applications that require both very thin circuits and low power consumption.

Facilitated by the mechanical, biocompatible, and electromechanical properties of circuits formed by patterning Au on a LMMPs-PDMS substrate, we designed and fabricated a flexible and stretchable neural electrode array with 8 channels (Figures 5D and 5E) for the *in vivo* identification of epilepsy by monitoring the signals of electrocorticogram (ECoG). A rat had a craniectomy and durotomy performed after being anesthetized, a 4 × 6 mm region of the right cortex was exposed and covered by the neural electrode, as shown in Figure 5F. The electrode array can conformally match the targeted cortical surface due to its high flexibility and stretchability. Figure 5G shows the ECoG signals recorded by one channel of the neural electrode when the rat was in normal and epileptic states, respectively. Signals recorded by other channels are shown in Figure S19. Compared with the normal state, an increased amplitude of the local field potential of the epileptic state can be clearly observed using our neural electrode. Also, attributed to the brain synchronic discharge induced by epilepsy, there is an associated increase in high-frequency energy, as shown in the time-frequency spectrum. Our flexible conductor offers numerous advantages for ECoG signal monitoring. Compared to traditional electrodes made of rigid materials such as silicon, our flexible electrodes have much better conformality that can make them easy to maintain stationary positions relative to the neurons under movement, and it can also reduce the possibility of brain tissue inflammation or mechanical damage.[60–62] Compared with the reported LM-based implantable electrodes prepared by hand-operated injection method and additional electrochemical deposition process,[63,64] our electrodes prepared by depositing an Au film on the LMMPs-PDMS substrate offer high accuracy and batch-to-batch consistency. More importantly, for biosafety, our method avoids the leaking issue of LM, and the Au film has been proven to be clinically biocompatible. Overall, the reliable electromechanical properties of the neural electrode with IT architecture enable the electrode to record ECoG signals with a high-throughput spatio-temporal resolution that is capable of distinguishing the normal state and epileptic state. Besides, this

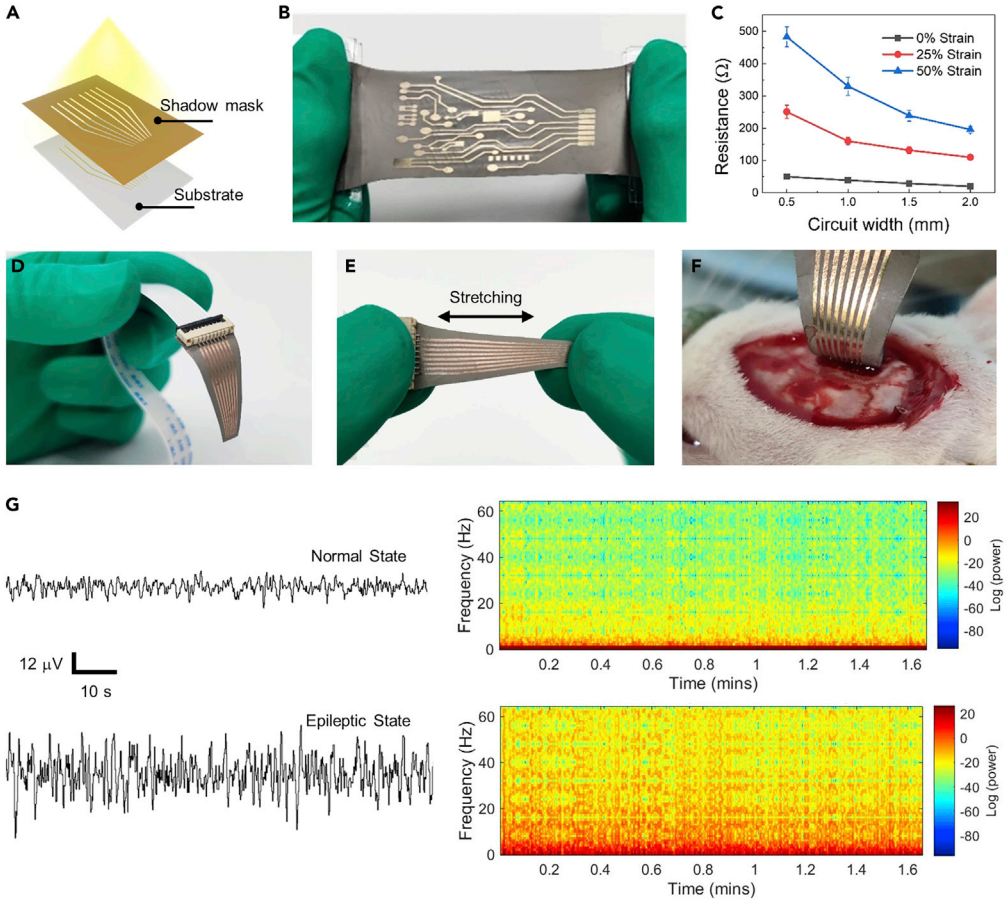

Figure 5. The method of directly patterning circuits on LMMPs-PDMS composite substrate and its application for monitoring signals of ECoG

(A) Patterning a specific circuit on the LMMPs-PDMS composite substrate using a PI shadow mask.

(B) Photograph of the patterned circuits.

(C) Electromechanical response of patterned 30 mm-length circuits with different widths under 0%, 25%, and 50% strain.

(D and E) Photos of the assembled neural electrode arrays under normal and stretched states, respectively.

(F) Intraoperative image of the neural electrode arrays for *in vivo* recording ECoG signals, showing the high flexibility of the electrode to be in contact with the cerebral cortex of the rat.

(G) ECoG signals of a healthy rat under normal state and epileptic state. The left picture is the local field potential trace and the right is the corresponding time-frequency spectrogram, showing an increment in high-frequency discharge for the epilepsy state. See also Figures S18 and S19.

neural electrode capable of monitoring epilepsy activity provides a new solution for brain-computer interfaces in relevant disease diagnosis.

Conclusion

In summary, we report a crack compensation strategy based on IT architectures for the fabrication of highly stretchable conductors by simply sputtering Au thin film on a LMMPs-PDMS substrate. The composite substrate prepared by mechanically mixing LM and PDMS not only improves the reliability of the ever-present fluid characteristic of LM but also increases the stretchability as compared with a PDMS substrate alone. In contrast to rigid metal particles, LMMPs with limited fluidity characteristics on the surface of the substrate can directly contact the Au film to act as deformable tunnels to compensate for cracks generated on the Au film. Compared with the Au film deposited on the PDMS substrate directly, the developed conductor with IT architectures can be easily stretched up to 260% strain with a negligible resistance change attributed to the compensation strategy. To demonstrate its practical applications, we applied the conductor to record the sEMG signals of six hand gestures, and machine learning-enabled hand gesture recognition was further

developed. In addition, stretchable circuits with specific patterns were fabricated to act as the neural electrode with 8 channels, which realized ECoG signals monitoring to distinguish the normal state and epileptic state of a rat. Therefore, our crack compensation strategy enabled by embedding LMMPs into PDMS substrate takes full use of the intrinsic properties of the electrical conductivity and flexibility of LM. The currently developed method significantly improves the stretchability of Au film-based flexible conductors, which not only provides a new way for the fabrication of high-performance stretchable conductors but also demonstrates great potential in the field of bioelectronics for *in vivo*/*vitro* applications.

Limitations of the study

Due to the difference in physical and chemical properties between metals and polymers, improving the adhesion between the Au film and the elastomeric substrate remains a challenge. There is a neglected improvement of the adhesion of Au film by using our proposed crack compensation strategy. Further efforts should be devoted to enhancing the adhesion of the Au film; one possible approach could be spin coating a very thin layer of conductive glue on the LMMPs-PDMS substrate before depositing the Au film.

STAR★METHODS

Detailed methods are provided in the online version of this paper and include the following:

- KEY RESOURCES TABLE
- RESOURCE AVAILABILITY
  - Lead contact
  - Materials availability
  - Data and code availability
- EXPERIMENTAL MODEL AND SUBJECT DETAILS
- METHOD DETAILS
  - Preparation of the PDMS-LMMPs substrate
  - Preparation of the stretchable conductors
  - Microstructure characterization and performance testing
- QUANTIFICATION AND STATISTICAL ANALYSIS
- ADDITIONAL RESOURCES

SUPPLEMENTAL INFORMATION

Supplemental information can be found online at https://doi.org/10.1016/j.isci.2022.105495.

ACKNOWLEDGMENTS

This work was supported by the financial supports from Shenzhen Science and Technology Program (KQTD20170809110344233, ZDSYS20190902093209795), Shenzhen Bay Laboratory (SZBL201906281005), the NSFC-Shenzhen Robotics Research Center Project (U2013207), the National Natural Science Foundation of China (81927804, 92163109, U1913601), and Fundamental Research Funds for the Central Universities (Grant No. HIT.OCEF.2021032).

AUTHOR CONTRIBUTIONS

G.Q. L. and X. M. proposed the project and conceived the idea. G.Q. L., X. M., and Z.Y. L. designed the experiments. Z.R. X., M. Y., J.P. H., J.J. W., S.H. L., F. H., H.F. L., Y.F. S., and B., performed the experiments. G.Q. L., X. M., M. Y., S.-Y. T., and B. analyzed the results. G.Q. L., X. M., S.-Y. T., Z.Y. L., and T. C. participated in writing the article.

DECLARATION OF INTERESTS

The authors declare no competing interests.

Received: July 22, 2022
Revised: October 4, 2022
Accepted: November 1, 2022
Published: December 22, 2022

REFERENCES

1. Ling, Y., An, T., Yap, L.W., Zhu, B., Gong, S., and Cheng, W. (2020). Disruptive, soft, wearable sensors. Adv. Mater. *32*, e1904664.

2. Zhu, M., Ji, S., Luo, Y., Zhang, F., Liu, Z., Wang, C., Lv, Z., Jiang, Y., Wang, M., Cui, Z., et al. (2022). A mechanically interlocking strategy based on conductive microbridges for stretchable electronics. Adv. Mater. *34*, e2101339.

3. Liu, Z., Wang, H., Huang, P., Huang, J., Zhang, Y., Wang, Y., Yu, M., Chen, S., Qi, D., Wang, T., et al. (2019). Highly stable and stretchable conductive films through thermal-radiation-assisted metal encapsulation. Adv. Mater. *31*, 1901360.

4. Koo, J.H., Kim, D.C., Shim, H.J., Kim, T.-H., and Kim, D.-H. (2018). Flexible and stretchable smart display: materials, fabrication, device design, and system integration. Adv. Funct. Mater. *28*, 1801834.

5. Chen, Y., Wu, Y., Mechael, S.S., and Carmichael, T.B. (2019). Heterogeneous surface orientation of solution-deposited gold films enables retention of conductivity with high strain-a new strategy for stretchable electronics. Chem. Mater. *31*, 1920–1927.

6. Cho, C., Kang, P., Taqieddin, A., Jing, Y., Yong, K., Kim, J.M., Haque, M.F., Aluru, N.R., and Nam, S. (2021). Strain-resilient electrical functionality in thin-film metal electrodes using two-dimensional interlayers. Nat. Electron. *4*, 126–133.

7. Petritz, A., Karner-Petritz, E., Uemura, T., Schäffner, P., Araki, T., Stadlober, B., and Sekitani, T. (2021). Imperceptible energy harvesting device and biomedical sensor based on ultraflexible ferroelectric transducers and organic diodes. Nat. Commun. *12*, 2399.

8. Nan, K., Kang, S.D., Li, K., Yu, K.J., Zhu, F., Wang, J., Dunn, A.C., Zhou, C., Xie, Z., Agne, M.T., et al. (2018). Compliant and stretchable thermoelectric coils for energy harvesting in miniature flexible devices. Sci. Adv. *4*, eaau5849.

9. Mechael, S.S., Wu, Y., Schlingman, K., and Carmichael, T.B. (2018). Stretchable metal films. Flex. Print. Electron. *3*, 043001.

10. Lim, H.R., Kim, H.S., Qazi, R., Kwon, Y.T., Jeong, J.W., and Yeo, W.H. (2020). Advanced soft materials, sensor integrations, and applications of wearable flexible hybrid electronics in healthcare, energy, and environment. Adv. Mater. *32*, e1901924.

11. Lambricht, N., Pardoen, T., and Yunus, S. (2013). Giant stretchability of thin gold films on rough elastomeric substrates. Acta Mater. *61*, 540–547.

12. Kim, J., Lee, M., Shim, H.J., Ghaffari, R., Cho, H.R., Son, D., Jung, Y.H., Soh, M., Choi, C., Jung, S., et al. (2014). Stretchable silicon nanoribbon electronics for skin prosthesis. Nat. Commun. *5*, 5747–5811.

13. Kim, D.-H., Ahn, J.-H., Choi, W.M., Kim, H.-S., Kim, T.-H., Song, J., Huang, Y.Y., Liu, Z., Lu, C., and Rogers, J.A. (2008). Stretchable and foldable silicon integrated circuits. Science *320*, 507–511.

14. Xu, S., Yan, Z., Jang, K.-I., Huang, W., Fu, H., Kim, J., Wei, Z., Flavin, M., McCracken, J., Wang, R., et al. (2015). Assembly of micro/nanomaterials into complex, three-dimensional architectures by compressive buckling. Science *347*, 154–159.

15. Mertens, J., Bowman, R.W., Willis, J.C., Robinson, A., Cotton, D., White, R., Seffen, K.A., and Baumberg, J.J. (2015). Scalable microaccordion mesh for deformable and stretchable metallic films. Phys. Rev. Appl. *4*, 044006.

16. Chen, C., Tao, W., Su, Y., Wu, J., and Song, J. (2013). Lateral buckling of interconnects in a noncoplanar mesh design for stretchable electronics. J. Appl. Mech. *80*, 041031.

17. Robinson, A.P., Minev, I., Graz, I.M., and Lacour, S.P. (2011). Microstructured silicone substrate for printable and stretchable metallic films. Langmuir *27*, 4279–4284.

18. Zhao, X., Yang, S., Sun, Z., Cui, N., Zhao, P., Tang, Q., Tong, Y., and Liu, Y. (2019). Enhancing the intrinsic stretchability of micropatterned gold film by covalent linkage of carbon nanotubes for wearable electronics. ACS Appl. Electron. Mater. *1*, 1295–1303.

19. Graudejus, O., Görrn, P., and Wagner, S. (2010). Controlling the morphology of gold films on poly (dimethylsiloxane). ACS Appl. Mater. Interfaces *2*, 1927–1933.

20. Chen, M., Yang, F., Chen, X., Qin, R., Pi, H., Zhou, G., and Yang, P. (2021). Crack suppression in conductive film by amyloid-like protein aggregation toward flexible device. Adv. Mater. *33*, e2104187.

21. Cordill, M.J., Paulitsch, M., Katsarelis, C., Putz, B., Lassnig, A., and Kennedy, M.S. (2022). Influence of interlayers on the interfacial behavior of Ag films on polymer substrates. Thin Solid Films *742*, 139051.

22. Pan, S., Liu, Z., Wang, M., Jiang, Y., Luo, Y., Wan, C., Qi, D., Wang, C., Ge, X., and Chen, X. (2019). Mechanocombinatorially screening sensitivity of stretchable strain sensors. Adv. Mater. *31*, e1903130.

23. Vandeparre, H., Liu, Q., Minev, I.R., Suo, Z., and Lacour, S.P. (2013). Localization of folds and cracks in thin metal films coated on flexible elastomer foams. Adv. Mater. *25*, 3117–3121.

24. Wu, X., Chen, H., Luo, X., Wang, D., Schaaf, P., and Zhang, G. (2021). Ultrasensitive strain sensors based on Cu-Al alloy films with voided cluster boundaries. Adv. Mater. Technol. *6*, 2100524.

25. Lee, Y., Kim, B.J., Hu, L., Hong, J., and Ahn, J.-H. (2022). Morphable 3D structure for stretchable display. BMC Wom. Health *22*, 51–57.

26. Hirsch, A., Michaud, H.O., Gerratt, A.P., de Mulatier, S., and Lacour, S.P. (2016). Intrinsically stretchable biphasic (solid-liquid) thin metal films. Adv. Mater. *28*, 4507–4512.

27. Dickey, M.D. (2017). Stretchable and soft electronics using liquid metals. Adv. Mater. *29*, 1606425.

28. Ma, Z., Huang, Q., Xu, Q., Zhuang, Q., Zhao, X., Yang, Y., Qiu, H., Yang, Z., Wang, C., Chai, Y., and Zheng, Z. (2021). Permeable superelastic liquid-metal fibre mat enables biocompatible and monolithic stretchable electronics. Nat. Mater. *20*, 859–868.

29. Liu, S., Shah, D.S., and Kramer-Bottiglio, R. (2021). Highly stretchable multilayer electronic circuits using biphasic gallium-indium. Nat. Mater. *20*, 851–858.

30. Tang, S.-Y., Tabor, C., Kalantar-Zadeh, K., and Dickey, M.D. (2021). Gallium liquid metal: the devil's elixir. Annu. Rev. Mater. Res. *51*, 381–408.

31. Markvicka, E.J., Bartlett, M.D., Huang, X., and Majidi, C. (2018). An autonomously electrically self-healing liquid metal-elastomer composite for robust soft-matter robotics and electronics. Nat. Mater. *17*, 618–624.

32. Yun, G., Tang, S.-Y., Zhao, Q., Zhang, Y., Lu, H., Yuan, D., Sun, S., Deng, L., Dickey, M.D., and Li, W. (2020). Liquid metal composites with anisotropic and unconventional piezoconductivity. Matter *3*, 824–841.

33. Yun, G., Tang, S.Y., Sun, S., Yuan, D., Zhao, Q., Deng, L., Yan, S., Du, H., Dickey, M.D., and Li, W. (2019). Liquid metal-filled magnetorheological elastomer with positive piezoconductivity. Nat. Commun. *10*, 1300.

34. Cao, W., Görrn, P., and Wagner, S. (2011). Modeling the electrical resistance of gold film conductors on uniaxially stretched elastomeric substrates. Appl. Phys. Lett. *98*, 212112.

35. Fassler, A., and Majidi, C. (2015). Liquid-phase metal inclusions for a conductive polymer composite. Adv. Mater. *27*, 1928–1932.

36. Zhang, M., Li, G., Huang, L., Ran, P., Huang, J., Yu, M., Yuqian, H., Guo, J., Liu, Z., and Ma, X. (2021). Versatile fabrication of liquid metal nano-ink based flexible electronic devices. Appl. Mater. Today *22*, 100903.

37. Bartlett, M.D., Fassler, A., Kazem, N., Markvicka, E.J., Mandal, P., and Majidi, C. (2016). Stretchable, high-k dielectric elastomers through liquid-metal inclusions. Adv. Mater. *28*, 3726–3731.

38. Liu, Z., Yu, M., Lv, J., Li, Y., and Yu, Z. (2014). Dispersed, porous nanoislands landing on stretchable nanocrack gold films: maintenance of stretchability and controllable impedance. ACS Appl. Mater. Interfaces *6*, 13487–13495.

39. Zhang, B., Lei, J., Qi, D., Liu, Z., Wang, Y., Xiao, G., Wu, J., Zhang, W., Huo, F., and

Chen, X. (2018). Stretchable conductive fibers based on a cracking control strategy for wearable electronics. Adv. Funct. Mater. *28*, 1801683.

40. Niklaus, M., Rosset, S., Dadras, M., Dubois, P., and Shea, H. (2008). Microstructure of 5keV gold-implanted polydimethylsiloxane. Scr. Mater. *59*, 893–896.

41. Rosset, S., Niklaus, M., Dubois, P., and Shea, H.R. (2009). Metal ion implantation for the fabrication of stretchable electrodes on elastomers. Adv. Funct. Mater. *19*, 470–478.

42. De Vivo, B., Lamberti, P., Spinelli, G., Tucci, V., Vertuccio, L., and Vittoria, V. (2014). Simulation and experimental characterization of polymer/carbon nanotubes composites for strain sensor applications. J. Appl. Phys. *116*, 054307.

43. Amjadi, M., Pichitpajongkit, A., Lee, S., Ryu, S., and Park, I. (2014). Highly stretchable and sensitive strain sensor based on silver nanowire elastomer nanocomposite. ACS Nano *8*, 5154–5163.

44. Alamusi, Hu, N., Fukunaga, H., Atobe, S., Liu, Y., and Li, J. (2011). Piezoresistive strain sensors made from carbon nanotubes based polymer nanocomposites. Sensors *11*, 10691–10723.

45. Lin, Y., Cooper, C., Wang, M., Adams, J.J., Genzer, J., and Dickey, M.D. (2015). Handwritten, soft circuit boards and antennas using liquid metal nanoparticles. Small *11*, 6397–6403.

46. Park, J.E., Kang, H.S., Baek, J., Park, T.H., Oh, S., Lee, H., Koo, M., and Park, C. (2019). Rewritable, printable conducting liquid metal hydrogel. ACS Nano *13*, 9122–9130.

47. Liu, S., Yuen, M.C., White, E.L., Boley, J.W., Deng, B., Cheng, G.J., and Kramer-Bottiglio, R. (2018). Laser sintering of liquid metal nanoparticles for scalable manufacturing of soft and flexible electronics. ACS Appl. Mater. Interfaces *10*, 28232–28241.

48. Cole, T., Khoshmanesh, K., and Tang, S.-Y. (2021). Liquid metal enabled biodevices. Adv. Intell. Syst. *3*, 2000275.

49. Yeo, W.H., Kim, Y.S., Lee, J., Ameen, A., Shi, L., Li, M., Wang, S., Ma, R., Jin, S.H., Kang, Z., et al. (2013). Multifunctional epidermal electronics printed directly onto the skin. Adv. Mater. *25*, 2773–2778.

50. Tian, L., Zimmerman, B., Akhtar, A., Yu, K.J., Moore, M., Wu, J., Larsen, R.J., Lee, J.W., Li, J., Liu, Y., et al. (2019). Large-area MRI-compatible epidermal electronic interfaces for prosthetic control and cognitive monitoring. Nat. Biomed. Eng. *3*, 194–205.

51. Jeong, J.W., Yeo, W.H., Akhtar, A., Norton, J.J.S., Kwack, Y.J., Li, S., Jung, S.Y., Su, Y., Lee, W., Xia, J., et al. (2013). Materials and optimized designs for human-machine interfaces via epidermal electronics. Adv. Mater. *25*, 6839–6846.

52. Inzelberg, L., Pur, M.D., Schlisske, S., Rödlmeier, T., Granoviter, O., Rand, D., Steinberg, S., Hernandez-Sosa, G., and Hanein, Y. (2018). Printed facial skin electrodes as sensors of emotional affect. Flex. Print. Electron. *3*, 045001.

53. Fang, Y., and Liu, H. (2014). Robust sEMG electrodes configuration for pattern recognition based prosthesis control. IEEE International Conference on Systems, Man, and Cybernetics (IEEE), pp. 2210–2215.

54. Zeng, X., Dong, Y., and Wang, X. (2020). Flexible electrode by hydrographic printing for surface electromyography monitoring. Materials *13*, 2339.

55. Xu, B., Akhtar, A., Liu, Y., Chen, H., Yeo, W.H., Park, S.I., Boyce, B., Kim, H., Yu, J., Lai, H.Y., et al. (2016). An epidermal stimulation and sensing platform for sensorimotor prosthetic control, management of lower back exertion, and electrical muscle activation. Adv. Mater. *28*, 4462–4471.

56. Jiang, Z., Nayeem, M.O.G., Fukuda, K., Ding, S., Jin, H., Yokota, T., Inoue, D., Hashizume, D., and Someya, T. (2019). Highly stretchable metallic nanowire networks reinforced by the underlying randomly distributed elastic polymer nanofibers via interfacial adhesion improvement. Adv. Mater. *31*, e1903446.

57. Chu, J.-U., Song, K.-I., Han, S., Lee, S.H., Kim, J., Kang, J.Y., Hwang, D., Suh, J.-K.F., Choi, K., and Youn, I. (2012). Improvement of signal-to-interference ratio and signal-to-noise ratio in nerve cuff electrode systems. Physiol. Meas. *33*, 943–967.

58. Hu, Y., Li, F., Li, H., and Liu, C. (2017). An enhanced empirical wavelet transform for noisy and non-stationary signal processing. Digit. Signal Process. *60*, 220–229.

59. Azhiri, R.B., Esmaeili, M., and Nourani, M. (2021). EMG-based feature extraction and classification for prosthetic hand control. Preprint at arXiv. https://doi.org/10.48550/arXiv.2107.00733.

60. Vince, V., Brelen, M.E., Delbeke, J., and Colin, I.M. (2005). Anti-TNF-alpha reduces the inflammatory reaction associated with cuff electrode implantation around the sciatic nerve. J. Neuroimmunol. *165*, 121–128.

61. Moran, D. (2010). Evolution of brain-computer interface: action potentials, local field potentials and electrocorticograms. Curr. Opin. Neurobiol. *20*, 741–745.

62. Xu, K., Li, S., Dong, S., Zhang, S., Pan, G., Wang, G., Shi, L., Guo, W., Yu, C., and Luo, J. (2019). Bioresorbable electrode array for electrophysiological and pressure signal recording in the brain. Adv. Healthc. Mater. *8*, e1801649.

63. Wang, S., Nie, Y., Zhu, H., Xu, Y., Cao, S., Zhang, J., Li, Y., Wang, J., Ning, X., and Kong, D. (2022). Intrinsically stretchable electronics with ultrahigh deformability to monitor dynamically moving organs. Sci. Adv. *8*, eabl5511.

64. Wen, X., Wang, B., Huang, S., Liu, T.L., Lee, M.S., Chung, P.S., Chow, Y.T., Huang, I.W., Monbouquette, H.G., Maidment, N.T., and Chiou, P.Y. (2019). Flexible, multifunctional neural probe with liquid metal enabled, ultra-large tunable stiffness for deep-brain chemical sensing and agent delivery. Biosens. Bioelectron. *131*, 37–45.

STAR★METHODS

KEY RESOURCES TABLE

REAGENT or RESOURCE	SOURCE	IDENTIFIER
Chemicals, peptides, and recombinant proteins		
EGaIn	Dingguan Technology	CAS: 37345-62-3
Polydimethylsiloxane Sylgard 184	Dow Corning	CAS: 9016-00-6
Phosphate buffered saline	Sigma Aldrich	Cat#806552
Dimethyl sulfoxide	Sigma Aldrich	CAS: 67-68-5
Calcein-AM, PI solutions	Baiaolaibo Inc.	Cat# SY0501
Chloral hydrate	Sigma Aldrich	CAS: 302-17-0
Penicillin	Sigma Aldrich	CAS: 87-08-1
Thiazolyl Blue Tetrazolium Bromide	Sigma Aldrich	CAS: 298-93-1
Experimental models: Organisms/strains		
Rat: Female, Sprague-Dawley	Guangdong Medical Experimental Animal Center	~250 g
HEK-293	Xiamen University	N/A
Software and algorithms		
Matlab	MathWorks	http://www.mathworks.com
Comsol	Comsol. Inc.	https://www.comsol.com

RESOURCE AVAILABILITY

Lead contact

Further information and requests for resources and reagents should be directed and will be fulfilled by the lead contact, Xing Ma (maxing@hit.edu.cn).

Materials availability

The study did not generate any unique reagents.

Data and code availability

- All data reported in this paper will be shared by the lead contact upon request.
- This paper does not report the original code.
- Any additional information requested to reanalyze the data reported in this paper is available from the lead contact upon request.

EXPERIMENTAL MODEL AND SUBJECT DETAILS

All animal procedures and experiments were performed following the guidance of the Institutional Animal Care and Use Committee at Harbin Institute of Technology (Shenzhen). Adult female Sprague-Dawley rats (~250 g) obtained from Guangdong Medical Experimental Animal Center were subjected to this experiment. The rats were housed under a 12/12 h light/dark cycle for 7 days and provided *ad libitum* food and water. The rats lived in the clean room with constant temperature (~25°C) and humidity (60%) for 7 days to adapt to the environment prior to the experiment. The rats were anesthetized using chloral hydrate (CAS No. 302-17-0, 350 mg/kg) and fixed using a stereotaxic frame. Then 4 × 6 mm elliptical region of the brain surface over the motor cortex was exposed using a surgical drill and moved away from the bone flap. Finally, the neural electrode was positioned over the exposed cortex and the ECoG was detected. After the normal ECoG remained stable for 10 minutes, penicillin at a 2 million units/kg dose was injected in the intraperitoneal to induce a seizure and record it after about half an hour. The ECoG was detected using a 64-channel electroencephalograph system (Nation Inc., Shanghai, China) with a 128 Hz sampling rate. The recorded signals were performed using a custom-designed Matlab code.

HEK-293 cells were used to examine the cytotoxicity of the prepared stretchable conductor. 5×10^4 HEK-293 cells in 100 μm medium were seeded in 96-well plates and cultured in a humid incubator for 24 h. The PDMS, EGaIn, and stretchable conductor were mechanically crushed into microparticles in phosphate buffered saline (PBS) solution, and then they were diluted into the medium by the concentration of 100 μg/mL, respectively. After the cells were incubated for another 5 h to finish the update and then remove the previous medium, 100 μL medium containing 10 μL 3-(4,5-dimethylthiazo1-2-yl)-2,5-diphenyltetrazoliumbromide (MTT) solution was added to every well. Then, the medium was removed after cells were incubated for 5 h, and 100 μL dimethylsulfoxide (DMSO) was added to each well. The absorption at 570 nm reflects the cell metabolic activity, and the cell viability was calculated by the absorption ratio between the treatment and control groups. For live-dead cell staining evaluation, 1 mL HEK-293 (5×10^4) were incubated in a petri dish for 24 h. Then, 1 mL PDMS, EGaIn, and stretchable conductor in PBS solution with 100 g/mL concentration was added to the culture medium, respectively. After being incubated for 5 h, the medium was removed and the petri dish was washed with PBS solution 3 times. After that, the cells were dispersed in 5 mL 1× assay buffer, stained with AM (2 mM) and PI (1.5 mM) solution, and overshadowed for 15 min at 37°C. Since the stained solution was removed and the samples were washed with PBS solution for 3 times, the fluorescence of the stained cells was observed using confocal laser scanning microscopy (CLSM) with 488 nm and 561 nm excitation, respectively. Furthermore, all samples were cultured at 37°C in the incubator with 5% CO_2.

METHOD DETAILS

Preparation of the PDMS-LMMPs substrate

Polydimethylsiloxane (PDMS, Sylgard 184, Dow Corning) was prepared by mixing prepolymer and cross-linker at a weight ratio of 10:1. Eutectic Ga-In alloy (EGaIn, 75.5 wt.% Ga and 24.5 wt.% In, Dingguan Metal Technology Co., Ltd) was then mixed with PDMS using an electric mixer (LC-ES series, Lichen Technology Co., Ltd) for 3 min. For making a composite with liquid metal microparticles (LMMPs) of 7.5 μm diameter on average and 40 vol.% content, PDMS and EGaIn were mixed at a volume ratio of 3:2 and stirred using a stirring stick (diameter of 30 mm) for 5 min at 1200 RPM. For making a composite with LMMPs of 3.5 μm diameter on average and 40 vol.% content, PDMS and EGaIn were mixed at a volume ratio of 2:3 and stirred using a stirring stick (diameter of 30 mm) for 5 min at 1500 RPM. Next, an extra 20 vol.% PDMS was added to lower the volume fraction of LMMPs. The mixture was stirred for an extra 3 min until PDMS and LMMPs were mixed uniformly. The composite with 20 vol.% of LMMPs was prepared by adding an extra 20 vol.% PDMS into the mixture with 40 vol.% of LMMPs. After mixing the two components of EGaIn and PDMS, air bubbles within the composite were removed by vacuuming the uncured mixture for 15 min.

For the convenient characterization of the microstructure of the LMMPs-PDMS composite shown in Figure 2, a very thin layer of the composite was spin-coated on the surface of a PDMS substrate at 5,000 RPM for 30 s. For the conductors shown in Figures 3, 4, and 5, the substrates were prepared in two steps. Preparing a cured PDMS-LMMPs composite substrate firstly, and then spin coating a very thin layer LMMPs-PDMS composite with 5,000 RPM for 30 s on this cured composite substrate.

Preparation of the stretchable conductors

After the PDMS-LMMPs composite was cured at 70°C for 3 h in a petri dish. A 40-nm-thick gold (Au) film was deposited through a pre-patterned polyimide film mask using an SBC-12 ion sputtering apparatus (Kyky Technology Co., Ltd) with 8 mA current for 210 s, and the thickness of the Au film can be regulated by the sputtering time. Then, the patterned stretchable conductor was cut using a knife and peeled off from the petri dish.

Microstructure characterization and performance testing

Back-scattered electron (BSE) images for microstructure characterization of the LMMPs-PDMS composite and in-situ observation of the stretched conductor were performed using a Phenom XL scanning electron microscope equipped with a tensile sample holder. The surface morphology of the LMMPs-PDMS composite was characterized by a Sensofar 3D optical profilometer S neox. The thickness test of PDMS film on LMMPs was carried out by force-displacement measurement in the air using Bruker Dimension FastScan atomic force microscopes (AFM). We used In alloy to replace the EGaIn to fabricate the composite for force-displacement measurement. Firstly, the In alloy was heated at 200°C to melt, and then the prepolymer of PDMS was added and stirred at 1,200 rpm for 5 min. The cross-linker of PDMS should be added after

the composite cool down to room temperature. Therefore, the composite with solid-state metal particle fillers and a soft polymer matrix was prepared to measure the thickness of the PDMS film coated with particles. The resistance-strain response was carried out using a SHIMADZU AGS-X machine equipped with a multi-meter (Keithley, 2010).

QUANTIFICATION AND STATISTICAL ANALYSIS

Histogram Statistics are given with error bars calculated from at least 5 sets of independent experiments. The simulation data is produced by COMSOL software. Figures shown in the main text were produced by Origin and Microsoft PowerPoint from the raw data.

ADDITIONAL RESOURCES

Any additional information about the simulation and data reported in this paper is available from the lead contact on request.